RSC Advances

ROYAL SOCIETY OF CHEMISTRY

www.rsc.org/advances

Graphic Abstract

The size effect of Pt nanoparticles on detection of arsenic is clarified and the phenomenon is explained by anodic oxygen-transfer reactions and binding energy.

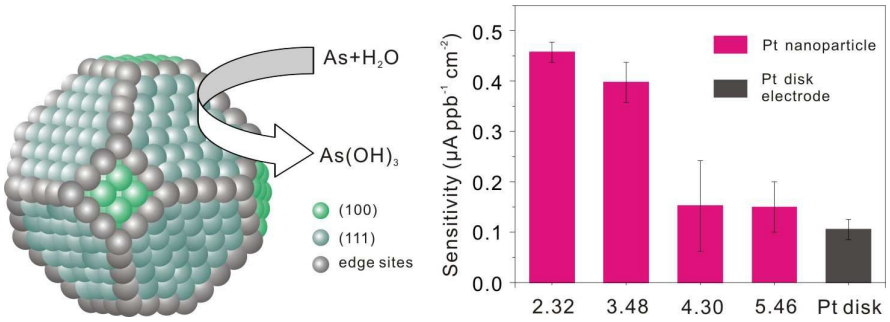

The size effect of Pt nanoparticles: A new route to improve sensitivity in electrochemical detection of As(III)

Dong-Dong Han,[1, 2] Zhong-Gang Liu,[1, 2] Jin-Huai Liu[2] and Xing-Jiu Huang*[1, 2]

[1]Department of Chemistry, University of Science and Technology of China, Hefei 230026, PR China

[2]Nanomaterials and Environmental Detection Laboratory, Hefei Institutes of Physical Science, Chinese Academy of Sciences, Hefei 230031, PR China

*Corresponding author: X.J.Huang

Tel: +86-551-5591142; Fax: +86-551-5592420;

E-mail: xingjiuhuang@iim.ac.cn (X.J.H).

Abstract

In this work, we demonstrate a size-dependent effect of Pt nanoparticles ranging 2-5 nm on the electrochemical behavior toward arsenic [As(III)]. This work presents the stripping voltammetry for sensitive identification of As(III) using four types of platinum nanoparticles for the first time, the sizes of which are 2.3, 3.5, 4.3 and 5.5 nm. Anodic oxygen-transfer reactions are expected to explain the interaction between As(III) and different size Pt nanoparticles for scientific understanding of the size effect on stripping voltammetry. We report that surface sites of Pt are made up of {111}, {100} facts and the edges. The percentage of the edges decreases with the increase of the particle size, while the percentage of {111}, {100} sites increases. The binding energy of the edge sites is higher than that of {111}, {100} facts. As a result, the desorption of the intermediates during the electrochemical process is easier on the edge sites. Therefore, the sensitivity of detection of As(III) is higher on the edge sites than on the {111} and {100} sites.

Keywords: size effect; platinum nanoparticles; anodic oxygen-transfer reactions; arsenic; stripping voltammetry.

Introduction

To date, much attention has been paid on the exploration of nanomaterials (especially, gold, platinum, etc.) modified electrodes for electrochemical detection of trace levels of arsenic, because it has a detrimental effect on human health and a great hazard to environment[1-4]. Arsenic is a poisonous chemical widely distributed all over the world and exists in four valency states: -3, 0, +3, and +5[5]. In ground waters, Arsenite [As(III)] is the general form in reducing conditions and arsenate [As(V)] is dominantly the stable form in oxygenated environments. Both of them have contributed greatly to many health problems such as skin lesions, keratosis (skin hardening), lung cancer, and bladder cancer[6]. It is reported that As(III) is 25~60 times more toxic than As(V)[7]. Therefore, it is urgent to find an accurate, fast, and sensitive method to detect and monitor this pollutant in drinking water.

To solve this problem, varieties of methods, such as inductively coupled plasma mass spectrometry (ICPMS)[8], graphite furnace atomic absorption spectrometry[9], and hydride generation atomic fluorescence spectrometry[10], can be used. Nevertheless, these techniques require expensive instruments, high operating cost, and well trained technicians to conduct the measurements[11]. On the contrary, electrochemical detection techniques may provide an promising alternative due to low-cost instrumentation and ease of portability. However, the sensitivity of electrochemical detection techniques is low. Thus, a lot of studies focus on the electrochemical methods and electrode nanomaterials to improve the sensitivity. Among all kinds of electrochemical methods, including cathodic stripping voltammetry (CSV), anodic stripping voltammetry(ASV)

and differential pulse anodic stripping voltammetry (DPASV), ASV is the most promising due to its high sensitivity, large linear range and low limit of detection (LOD)[12].

Due to the versatile and important properties of nanomaterials including large specific surface area, improved mass transport, and catalytic properties, these metal nanoparticles are gaining popularity. These properties can make the reagent have more area, lower resistance and lower energy to react. Therefore, different electrode nanomaterials, especially Hg, Au, Pt, were used to detect arsenic in many reports. Hg suffers from toxicity and the limited solubility of arsenic, although, it has a high sensitivity toward many pollution. Au and Pt are widely used, however, they suffer from lengthy analysis time, poor response precision and stability[13]. Compared With Au, Pt nanomaterial has a better catalyze ability in methanol oxidation reaction, oxygen reduction and electrocatalytic activity.[14-17] Thus, various kinds of Pt-based electrodes, such as Pt nanoparticle[18], Pt nanotube[19], Pt nanoflower[20], have been conducted to improve analytical performance.

Despite great success, these studies generally focused on a good analytical performance. Actually, nanomaterial processes many unique properties, such as crytal plane, crystal phase, small size effect, and so on. A serial of excellent results on the particle size effect of Pt nanoparticles have been reported in the field of catalysis. For example, Bell et al have investigated the effect of composition and metal particle size of Pt catalysts on ethane dehydrogenation[21]. Sung et al have reported that the particle size of Pt nanoparticles affects the catalytic reactions through making an alteration to

the value of the oxophilicity.[22] However, few studies have been carried out on the particle size effect in electrochemical detection, especially detection of arsenic. We would expect that different particle sizes of Pt nanoparticles would affect the detection of As(III). According to the result, we can synthesize the Pt nanoparticle in the best size to obtain the best analytical performance.

2. Materials and methods

2.1 Apparatus.

AutoLab computer-controlled potentiostat (EcoChemie, Utrecht, Netherlands) associated with the GPES software. A bare glass carbon electrode (GCE, diameter of 3 mm) or modified GCE was used as a working electrode; a platinum wire severed as a counter-electrode with a saturated Ag/AgCl electrode (Chen Hua Instruments Co., Shanghai, China) completing the cell assembly. All experiments were performed at a temperature of 293 ± 3K.

2.2 Chemical reagents.

Pt nanoparticles with an average particle size of 2.3 nm supported on Ketjen Black was purchased from Alfa Aesar, Tianjin, China. $CuSO_4$, H_2SO_4, K_2PtCl_4, HCl, HNO_3 and Nafion were all purchased from Sinopharm Chemical Reagent Co., Ltd., Shanghai, China. Double distilled water (MilliQ, specific resistivity >18 MΩ cm, S.A., Molsheim, France) was used throughout the experiment.

2.3 Electrode Fabrication.

Approximately 20 mg of Pt/C was added into a solvent consisting of 16 mL of water,

80μL of 5% Nafion, and 4 mL of isopropanol by ultrasonic for 10 min. 8 μL of suspension was deposited on the glass carbon electrode (GCE) polished with 0.3 and 0.05 μm alumina before modified.

2.4 Preparation of Pt nanoparticles in different size.

In our research, the Pt particle size was grown by layer-by-layer growth through a Cu-UPD-Pt replacement method. Underpotentially deposited (UPD) Cu was carried out in 0.5 M H_2SO_4 + 50 mM $CuSO_4$ solution. Then the electrode was immersed in a 5 mM K_2PtCl_4 + 0.5 M H_2SO_4 solution to displace the Cu with Pt.

2.5 Electrochemical Experiments.

The electrochemical characterization (cyclic voltammograms and electrochemical impedance spectra) were performed in a degassed solution with a high purity N_2 (Nanjing Special Gases Factory Co., Ltd.) containing 0.1 M KCl and 5 mM $K_3Fe(CN)_6$. The frequency range was from 0.1 Hz to 10000 Hz with signal amplitude of 5 mV, and the scan rate was 0.1 V s^{-1}.

The square wave anodic stripping voltammetry (SWASV) was measured in 0.5 M H_2SO_4 solution. The measurements were performed in the potential range from - 0.15 to + 0.60 V with a frequency of 15 Hz, amplitude of 25 mV, and a potential step of 4 mV. After each measurement, the electrode was regenerated by immersing in a stirring 0.5 M H_2SO_4 solution at + 0.8 V for 150 s. Then, the electrode was checked in the supporting electrolyte before the next measurement to ensure that it was renewed. All measurements were performed at room temperature.

2.6 Cu-UPD-Pt replacement method.

In an effort to control the platinum nanaoparticles size, we use a Cu-UPD-Pt replacement method[23] by layer-by-layer growth. An underpotentially deposited (UPD) Cu monolayer on a Pt substrate can be deposited from a 0.5 M H_2SO_4 + 50 mM $CuSO_4$ solution. The electrode covered with a Cu monolayer was immersed in a K_2PtCl_4 solution to the Cu with Pt.

3. Results and discussion

3.1 Characterization of the Pt nanoparticles.

The surface modified electrodes were firstly characterized by cyclic voltammetry (CV) (Fig. 1a). Since Pt/C nanoparticles consist of Pt and black carbon which are conductive material, they could be incorporated into the electrochemical system to facilitate the electron exchange between the electrochemical probe and the electrode and result in the enhanced conductivity of the matrices. Thus, the anodic and catholic peaks increased at the modified electrode compared with the bare GCE. Enhanced electrochemical responses (EIS) of 5 mM $K_3Fe(CN)_6$ at the modified glassy carbon electrodes were also observed (red line in Fig. 1b). In EIS, the semicircle diameter of the Nyquist diagram is equal to the surface electron transfer resistance (R_{et}). The immobilization of Pt/C nanoparticles on the electrode surface can change the R_{et} value. The obtained result further indicates that the Pt/C nanoparticles have been assembled onto the GCE surface and enhance the electron transfer between the electrolyte and the electrode.

Then we seek to optimize the experimental conditions (e.g. deposition potential,

deposition time and supporting electrolytes) for the determination of 1 ppm As(III) using Square wave anodic stripping voltammetry (SWASV). We compared the anodic peak current for As(III) obtained in three different supporting electrolytes: 0.5 M H_2SO_4 solution, 1 M HCl solution and 1 M HNO_3 solution (Fig. 2c). As it is clearly shown, the strongest response is obtained in H_2SO_4 solution. Therefore, the 0.5 M H_2SO_4 solution is selected as a supporting electrolyte for further optimization. In SWASV analysis, the application of suitable deposition potential is significant to achieve the best sensitivity. Thus the effect of the deposition potential on the peak current after 90 s accumulation is studied in the potential range from - 0.15 V to 0.1 V in 0.5 M H_2SO_4 solution. Fig. 2a plots the stripping peak current of As(III) against the deposition potential at the given conditions, which increases when the deposition potential shifts from 0.1 V to - 0.15 V. At more negative potential than - 0.15 V, however, the appearance of hydrogen is observed. Thus, we choose - 0.15 V as the optimal deposition potential for the subsequent stripping experiment. Also, the deposition time would affect the amount of analytes accumulated onto electrode surface, which further affected the detection limit and the sensitivity. As a result, the different deposition time was also studied in this work (Fig. 2b). As expected, the stripping peak currents for As(0) to As(III) enhances significantly with the increase of the deposition time varying from 30 up to 90 s, due to the increased amount of analytes onto the modified electrode surface. Then, a slower increase is obtained when further increasing the deposition time. Therefore, 90 s is chosen as accumulation time for further detection of As(III).

The different-sized Pt nanoparticles are synthesized through a Cu-UPD-Pt replacement method[23] by layer-by-layer growth. The underpotential deposition (UPD) phenomenon occurs in the first stage of electrochemical heteroepitaxial growth for many systems. During the initial stages of metal deposition, the electrochemical heteroepitaxial growth of two-dimensional single-crystal metal film can be observed. From the CVs showed in Fig. 3, it represents that at the Pt/C modified electrode the UPD-Cu occurs in a wide potential region from 0.8 V to 0.1 V. Thus, we believe the Cu monolayer synthesized at a potential of 0.13 V. To ensure UPD-Cu to take place completely, the electrode was kept at 0.13 V for 6 min. Then, the electrode covered with a Cu monolayer was immersed in a 5.0 mM K_2PtCl_4 + 0.5 M H_2SO_4 solution for about 5 min to displace the Cu with Pt. To avoid the interference of metal ions (Cu, Pt), the electrode was cleaned with water and cycled 50 cycles in N_2 saturated H_2SO_4 solution. At last, a final CV was recorded at 50 mV s^{-1} for electrochemical active areas (ECAs) calculation. This process was repeated on the electrode to increase the size of Pt layers and characterize their electrochemical behaviors. As we repeat this progress, the Pt layers have been added to the Pt particle and result in the growth of the particle. When we compare the sensitivity of different size particle, the ECAs are taken into consideration to eliminate of affecting elements, such as the change of the amount of platinum present and the surface area of the nanoparticle. Fig. 4 shows the typical TEM images of Pt/C after Pt depositing. The average particle sizes are 2.3, 3.5, 4.3, and 5.5 nm, corresponding to the as synthesized (Fig. 4a), after depositing 3 layers (Fig. 4b), after depositing 6 layers (Fig. 4c) and after depositing 9 layers (Fig. 4d) Pt particles,

respectively. Obviously, the Pt nanoparticles size increases as the repetition of Cu-UPD-Pt replacement procedure. That is confirmed by Fig. 5a, which shows the cyclic voltammograms of Pt/C for as synthesized and after depositing three, six, and nine layers of Pt. As it is shown, the hydrogen adsorption and desorption current density increases significantly with the increase of the Pt particles size. According to Fig. 5a, the ECAs are calculated by integrating the hydrogen adsorption charges assuming 220 μC cm^{-2} [24]. The measured ECAs are larger than the area of GCE. This phenomenon can be explained by the fact that the Pt nanoparticles were not signal layer dispersed on the electrode but several layers supported by black carbon. Fig. 5b shows that the ECAs increase obviously, as the size of nanoparticles increases. The obvious increase of ECAs is caused by the enlargement of the Pt nanoparticles surface areas which have a connection with the square of radius (R^2).

3.2 SWASV response toward detection of As(III).

Prior to discuss the electrochemical performance of Pt nanoparticles toward As(III), the experimental parameters (deposition potential, deposition time, supporting electrolytes) are firstly explored (Fig. 2). Under the optimal experimental conditions, Pt/C nanoparticles in different size modified GCEs are applied to the detection of the target As(III) by SWASV. Under the optimal experimental conditions, Pt/C nanoparticles in different size modified GCE is applied to the detection of the target As(III) by SWASV. As it is shown in Fig. 6, the linearity of peak current versus As(III) up to the concentration of 1000 ppb is obtained, with the sensitivity of the electrode 0.356 (2.3 nm) , 0.318 (3.5 nm), 0.169 (4.3 nm), 0.257 (5.5 nm) μA ppb^{-1}

(Inset), respectively. Fig. 8a displays SWASV response of Pt nanoparticles in different size modified GCE and Pt disk electrode for analysis of 500 ppb As(III). Obviously, the stripping peaks of Pt nanoparticles are significantly higher than that of Pt disk electrode. When the size of Pt nanoparticles increases from 2.3 nm to 4.3 nm, the stripping peaks decrease gradually. While the diameter is 5.5 nm, the peak increases, and this may be caused by the increase of Pt loaded on the surface of nanoparticles. After considering the ECAs, we find the sensitivity for detection of As(III) increased as the nanoparticles size decrease, as shown in Fig. 8b. The sensitivity for the Pt nanoparticles in 2.3 nm is about 3-fold of that for the Pt nanoparticles in 5.5 nm and 7-fold of that for the pt disk (Fig. 7). This phenomenon maybe connected with the active sites the particle explored. According to Krista Shoemaker et al's study, in which the size-dependent activity of the oxygen reduction on the particles is studied, surface sites of platinum are made up of {111}, {100}facts and the edges. The percentage of the edges decreases with a increase in particle size, while the percentage of {111},{100} sites increases[14]. Thus, the edge sites contributed greatly to the sensitivity of the detection for As(III).

3.3 Interference study.

It is a challenge to detect As(III) in the real sample without interference as a result of the other metal ions coprecipitated, especially Cu(II). Therefore Cu(II) is chosen for interference study. Fig. 9a shows the SWASV response obtained at Pt/C modified electrode for different concentration of As(III) in the presence of Cu(II) (1 ppm). The striping signal obtained for Cu(II) (0.1 V) is almost invisible, while the peak for As(III)

increase gradually. In the presence of Cu(II), the obtained sensitivity was 0.268 μA ppb^{-1}. However, in the absence of Cu(II), the obtained sensitivity (0.356 μA ppb^{-1}) is about 1/2 higher. In addition, when we fix the concentration of As(III), the loss on arsenic signal as the concentration of Cu(II) increased is provided in Fig. 9b and Fig. 9c. The decrease in sensitivity in the presence of Cu(II) can be attributed to the formation of intermetallic compounds (Cu_3As_2) and the competition by the Cu(II) for deposition sites. To solve this problem, more attention is needed.

3.4 Reasonable mechanism.

The electroanalysis of As(III) is recognized as an anodic oxygen-transfer reaction (Equation (1)) in which oxygen is transferred from H_2O to the oxidation product(s) (Equation (4))[18, 25-26]. Adsorbed hydroxyl radicals (PtOH)[27], the intermediate state of oxygen in the process of transfer from H_2O to As(0), may generate at the first step (Equation (2)) in the O-transfer reactions[28] and convert to the inactive oxide (PtO) (Equation (3))[27], which passivate the Pt surface for further detection of As(III)[29].

$$As + 3H_2O \rightarrow As(OH)_3 + 3H^+ + 3e^- \quad (1)$$

$$Pt + H_2O \rightarrow Pt(OH) + H^+ + e^- \quad (2)$$

$$Pt(OH) \rightarrow PtO + H^+ + e^- \quad (3)$$

$$Pt\text{-}As + 3H_2O \rightarrow Pt + As(OH)_3 + 3H^+ + e^- \quad (4)$$

Among all these sites, the binding energy of the edge sites is higher than that of {111}, {100} facts[14]. Thus it is easier for {111}, {100} sites to form PtOH. But it is more possible for PtOH to convert to PtO passivating the detection of As(III), as a result of a stronger Pt-O bond at these sites[30]. Therefore, as the increase of the

percentage of the edge sites, the sensitivity increases.

$$As(0)\ (ads) \rightarrow As(I)\ (aq) + e^- \qquad (5)$$

$$As(I)\ (aq) \rightarrow As(II)\ (aq) + e^- \qquad (6)$$

$$As(II)\ (aq) \rightarrow As(III)\ (aq) + e^- \qquad (7)$$

For the anodic oxygen-transfer reaction, the extremely high reactivity of the fact hinders reaction by blocking the active sites with strong adsorbed intermediates, while the extremely low reactivity impedes the dissociation of H-O bond and charge transfer[14]. Besides, the oxidation of As(0) is a multiple-step**,** multiple-electron electrochemical reaction.[23] According to Richard G. Compton et al's study, the transfer of the last accepted electron (Equation (7)) is the rate-determining step. Therefore, whether there is enough sites for the As(II) to adsorb is urgent for the detection. During the electrochemical process, the intermediates generate during the reaction (such as As(I))[26] may adsorb at the lower binding energy sites such as the {111}, {100} sites and further hinder the adsorption of As(II). It may indicate that the rate-determining step of the anodic oxygen-transfer reactions desorption of the intermediates during the electrochemical process. According to anodic oxygen-transfer reaction, we find the desorption of the intermediates and the formation of the inactive oxide on the surface of Pt nanoparticles may significantly affect the sensitivity of the detection of As(III). To clarify this effect, more studies are needed.

4. Conclusion

In the present work, the size of the platinum nanoparticles is increased through a Cu-UPD-Pt replacement method by layer-by-layer growth. Then, the ECAs are calculated by integrating the hydrogen adsorption in H_2SO_4 solution. After considering the ECAs, we have demonstrated that the platinum size has an effect on the detection of As(III). As the size of Pt nanoparticles increases from 2.3 to 5.5 nm, the sensitivity decreases, which is caused by the change of the binding energy. The extremely low binding energy of the surface impedes reaction by blocking the active sites with strong adsorbed intermediates and with the formation of the inactive PtO during the anodic oxygen-transfer reaction. More importantly, this work presents an important insight into a new route to realize the improved sensitivity in electrochemical sensing of As(III) through the change of the particle size.

Acknowledgements

This work was supported by the National Key Scientific Program-Nanoscience and Nanotechnology (No. 2011CB933700), National Natural Science Foundation of China (No. 21103198, 21073197, and 90923033). X.J.H. acknowledges the One Hundred Person Project of the Chinese Academy of Sciences, China, for financial support.

References

1. Rahman, M. R.; Okajima, T.; Ohsaka, T., Selective detection of As (III) at the Au (111)-like polycrystalline gold electrode. *Anal Chem* **2010,** *82* (22), 9169-9176.

2. Hrapovic, S.; Liu, Y.; Luong, J. H., Reusable platinum nanoparticle modified boron doped diamond microelectrodes for oxidative determination of arsenite. *Anal Chem* **2007,** *79* (2), 500-507.

3. Mandal, B. K.; Suzuki, K. T., Arsenic round the world: a review. *Talanta* **2002,** *58* (1), 201-235.

4. Wu, Y.; Zhan, S.; Wang, F.; He, L.; Zhi, W.; Zhou, P., Cationic polymers and aptamers mediated aggregation of gold nanoparticles for the colorimetric detection of arsenic(iii) in aqueous solution. *Chem Commun* **2012,** *48* (37), 4459-4461.

5. Smedley, P. L.; Kinniburgh, D. G., A review of the source, behaviour and distribution of arsenic in natural waters. *Appl Geochem* **2002,** *17* (5), 517-568.

6. Majid, E.; Hrapovic, S.; Liu, Y. L.; Male, K. B.; Luong, J. H. T., Electrochemical determination of arsenite using a gold nanoparticle modified glassy carbon electrode and flow analysis. *Anal Chem* **2006,** *78* (3), 762-769.

7. Munoz, E.; Palmero, S., Analysis and speciation of arsenic by stripping potentiometry: a review. *Talanta* **2005,** *65* (3), 613-620.

8. Yan, X. P.; Kerrich, R.; Hendry, M. J., Determination of (ultra)trace amounts of arsenic(III) and arsenic(V) in water by inductively coupled plasma mass spectrometry coupled with flow injection on-line sorption preconcentration and separation in a knotted reactor. *Anal Chem* **1998,** *70* (22), 4736-4742.

9. Aggett, J.; Kriegman, M. R., The Extent of Formation of Arsenic(Iii) in Sediment Interstitial Waters and Its Release to Hypolimnetic Waters in Lake Ohakuri. *Water Res* **1988,** *22* (4), 407-411.

10. Yin, X. B.; Yan, X. P.; Jiang, Y.; He, X. W., On-line coupling of capillary electrophoresis to hydride generation atomic fluorescence spectrometry for arsenic speciation analysis. *Anal Chem* **2002,** *74* (15), 3720-3725.

11. Stuart, B. H.; Thomas, P. S., Xylene swelling of polycarbonate studied using Fourier transform Raman spectroscopy. *Spectrochim Acta A* **1995,** *51* (12), 2133-2137.

12. Dai, X.; Nekrassova, O.; Hyde, M. E.; Compton, R. G., Anodic stripping voltammetry of arsenic(III) using gold nanoparticle-modified electrodes. *Anal Chem* **2004,** *76* (19), 5924-5929.

13. Song, Y.; Swain, G. M., Development of a method for total inorganic arsenic analysis using anodic stripping voltammetry and a Au-coated, diamond thin-film electrode. *Anal Chem* **2007,** *79* (6), 2412-2420.

14. Shao, M. H.; Peles, A.; Shoemaker, K., Electrocatalysis on Platinum Nanoparticles: Particle Size Effect on Oxygen Reduction Reaction Activity. *Nano Lett* **2011,** *11* (9), 3714-3719.

15. Xia, B. Y.; Wu, H. B.; Wang, X.; Lou, X. W., One-Pot Synthesis of Cubic PtCu3 Nanocages with Enhanced Electrocatalytic Activity for the Methanol Oxidation Reaction. *J Am Chem Soc* **2012,** *134* (34), 13934-13937.

16. Xia, B. Y.; Ng, W. T.; Wu, H. B.; Wang, X.; Lou, X. W., Self-Supported Interconnected Pt Nanoassemblies as Highly Stable Electrocatalysts for Low-Temperature Fuel Cells. *Angew Chem Int Edit* **2012,** *51* (29), 7213-7216.

17. Xia, B. Y.; Wu, H. B.; Yan, Y.; Lou, X. W.; Wang, X., Ultrathin and Ultralong Single-Crystal Platinum Nanowire Assemblies with Highly Stable Electrocatalytic Activity. *J Am Chem Soc* **2013,** *135* (25), 9480-9485.

18. Dai, X.; Compton, R. G., Detection of As(III) via oxidation to As(V) using platinum nanoparticle modified glassy carbon electrodes: arsenic detection without interference from copper. *Analyst* **2006,** *131* (4), 516-521.

19. Xu, H.; Zeng, L. P.; Xing, S. J.; Shi, G. Y.; Chen, J. S.; Man, Y. Z.; Jin, L. T., Highly ordered platinum-nanotube arrays for oxidative determination of trace arsenic(III). *Electrochem Commun* **2008,** *10* (12), 1893-1896.

20. Jia, W. Z.; Su, L.; Lei, Y., Pt nanoflower/polyaniline composite nanofibers based urea biosensor. *Biosens Bioelectron* **2011,** *30* (1), 158-164.

21. Wu, J.; Peng, Z. M.; Bell, A. T., Effects of composition and metal particle size on ethane dehydrogenation over PtxSn100-x/Mg(Al)O (70 <= x <= 100). *J Catal* **2014,** *311*, 161-168.

22. Yoo, S. J.; Jeon, T.-Y.; Lee, K.-S.; Park, K.-W.; Sung, Y.-E., Effects of particle size on surface electronic and electrocatalytic properties of Pt/TiO2 nanocatalysts. *Chemical communications* **2010,** *46* (5), 794-796.

23. Zhang, J.; Mo, Y.; Vukmirovic, M. B.; Klie, R.; Sasaki, K.; Adzic, R. R., Platinum monolayer electrocatalysts for O-2 reduction: Pt monolayer on Pd(111) and on carbon-supported Pd nanoparticles. *J Phys Chem B* **2004,** *108* (30), 10955-10964.

24. Chen, D.; Tao, Q.; Liao, L. W.; Liu, S. X.; Chen, Y. X.; Ye, S., Determining the Active Surface Area for Various Platinum Electrodes. *Electrocatalysis* **2011,** *2* (3), 207-219.

25. Noskova, G. N.; Zakharova, E. A.; Kolpakova, N. A.; Kabakaev, A. S., Electrodeposition and stripping voltammetry of arsenic(III) and arsenic(V) on a carbon black-polyethylene composite electrode in the presence of iron ions. *J Solid State Electr* **2012,** *16* (7), 2459-2472.

26. Zhou, W. P.; Kibler, L. A.; Kolb, D. M., XPS study of irreversibly adsorbed arsenic on a Pt(111) electrode. *Electrochim Acta* **2004,** *49* (27), 5007-5012.

27. Shakkthivel, P.; Singh, P., Role of PtO on the oxidation of Arsenic (III) at Pt RDE in 1M H2SO4 and 1M Na2SO4 through Linear Sweep Voltammetry technique. *Int J Electrochem Sc* **2007,** *2* (4), 311-320.

28. Wei, Y.; Yang, R.; Zhang, Y.-X.; Wang, L.; Liu, J.-H.; Huang, X.-J., High adsorptive γ-AlOOH (boehmite)@ SiO2/Fe3O4 porous magnetic microspheres for detection of toxic metal ions in drinking water. *Chemical Communications* **2011,** *47* (39), 11062-11064.

29. Williams, D. G.; Johnson, D. C., Pulsed Voltammetric Detection of Arsenic(Iii) at Platinum-Electrodes in Acidic Media. *Anal Chem* **1992,** *64* (17), 1785-1789.

30. Xuan, T. T. P.; Le, T. T. T.; Tran, P. D.; Pham, B. V.; Tong, D. H.; Dang, M. C., Oxidation of a platinum microwire surface applied in glucose detection. *Advances in Natural Sciences: Nanoscience and Nanotechnology* **2010,** *1* (2), 025013.

Figure captions

Fig. 1 Cyclic voltammograms a) and Nyquist diagram of electrochemical impedance spectra b) for bare, Pt/C modified GCE in the solution of 5 mM $Fe(CN)_6^{3-/4-}$ containing 0.1 M KCl. Potential scan rate: 50 mV s^{-1}.

Fig. 2 Optimum experimental conditions: Influence of a) deposition potential; b) deposition time; and c) supporting electrolytes the voltammetric response of the Pt/C modified GCE. Data were evaluated by SWASV of 1 ppm As(III).

Fig. 3 CVs of Pt/C modified electrodes in 0.5 M H_2SO_4 (black line, -0.2~1.2 V), 0.5 M H_2SO_4 + 50 mM $CuSO_4$ (red line, 0.1~0.8 V); scan rate: 20 mV s^{-1}.

Fig. 4 TEM images of Pt particles supported on carbon black: a) as synthesized, b) after 3 layers deposition, c) after 6 layers deposition, and d) after 9 layers deposition, respectively. Insets in each panel are particle size distribution derived from TEM images. The mean particle sizes for a), b), c), and d) are 2.3, 3.5, 4.3, and 5.5 nm, respectively. Inset in panel b is a HRTEM image.

Fig. 5 a) CVs of Pt/C in different sizes in a N_2-saturated 0.5 M H_2SO_4 solution. Sweep rate 50 mV s^{-1}. b) The electrochemical active surface areas (ECAs) as a function of Pt particle size.

Fig. 6 a), c), e), g) Typical SWASV response of As(III) in different concentration ranges at Pt nanoparticles in different size modified GCE. b), f), g), h) Corresponding plots of peak current against As(III) linear calibration concentrations, respectively. SWASV conditions are identical to Fig. 2.

Fig. 7 SWASV response of Pt disk electrode for analysis of As(III) in different

concentration ranges without considering the ECAs.

Fig. 8 a) SWASV response of Pt nanoparticles in different size modified GCE and Pt disk electrode toward As(III) (C_0 = 500 ppb). b) Comparison of sensitivity toward As(III) at Pt nanoparticles modified GCE and Pt disk electrode.

Fig. 9 a) SWASV responses of the Pt/C modified GCE toward 0~1000 ppb As(III) in the presence of 1 ppm Cu(II) in 0.5 M H_2SO_4 solution, showing the interference of Cu(II) on the anodic peak currents of As(III). Inset is the plot of peak current versus the concentration of As(III) from 100~1000 ppb. The dotted line refers to the baseline. b) SWASV responses of the Pt/C modified GCE toward 0~10 ppm Cu(II) when the concentration of As(III) is 1000 ppb (1 ppm).

c) The corresponding loss of arsenic signal versus the changing concentration of Cu(II) in the presence of 1 ppm As(III).

Fig. 1

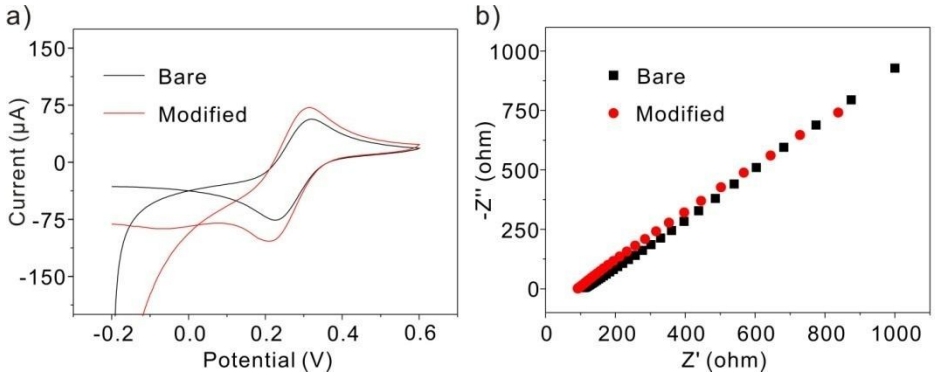

Fig. 2

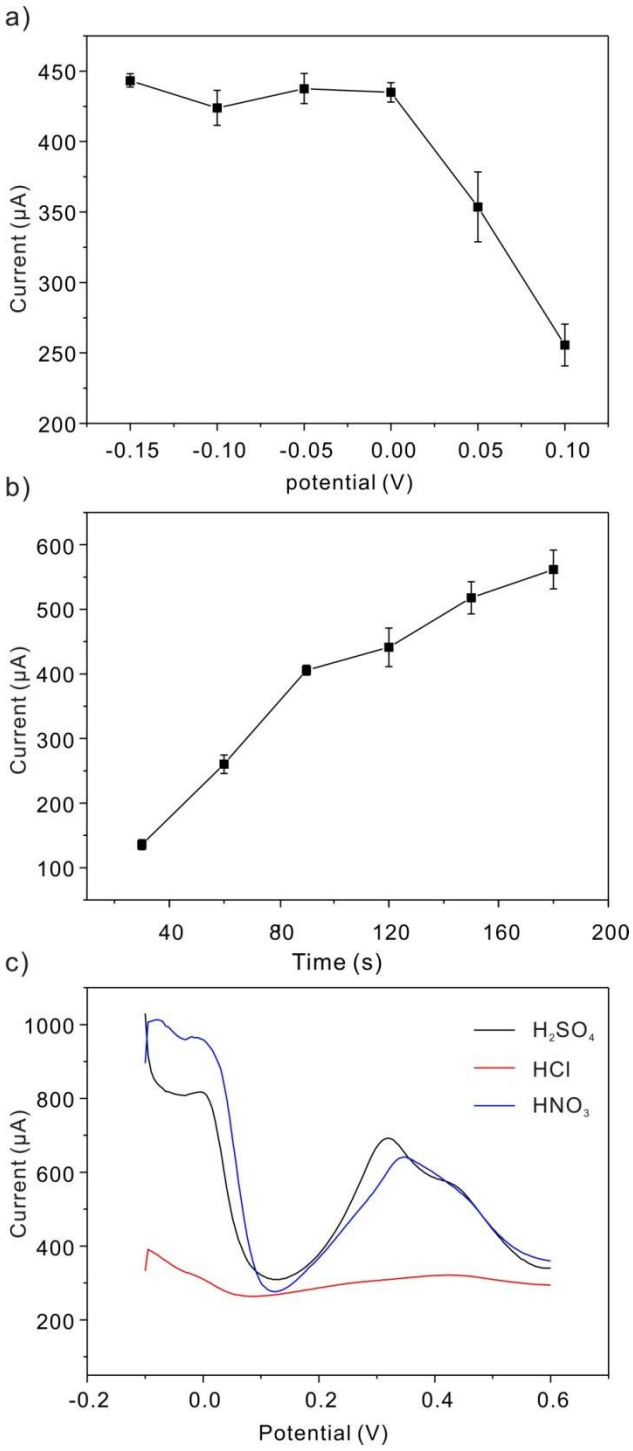

Fig. 3

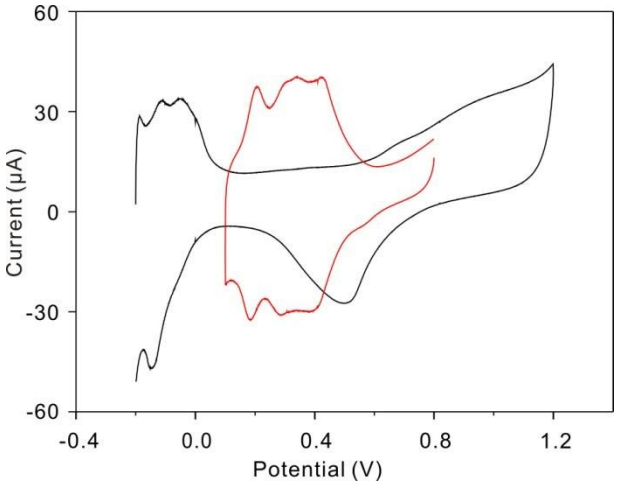

Fig. 4

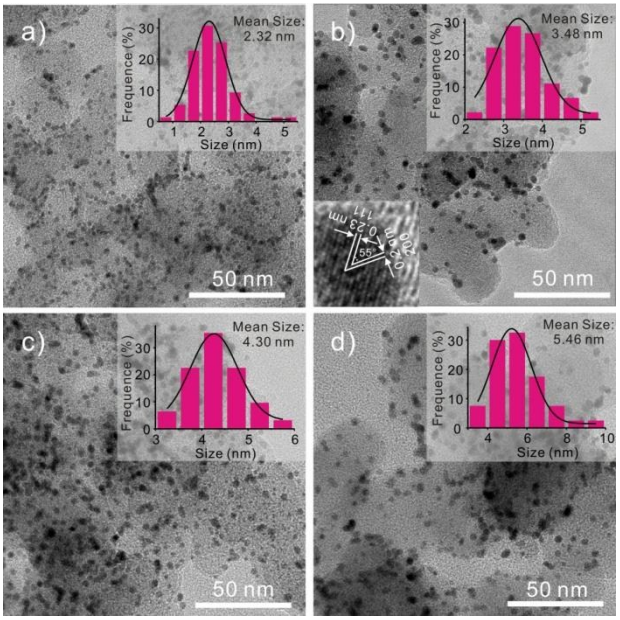

Fig. 5

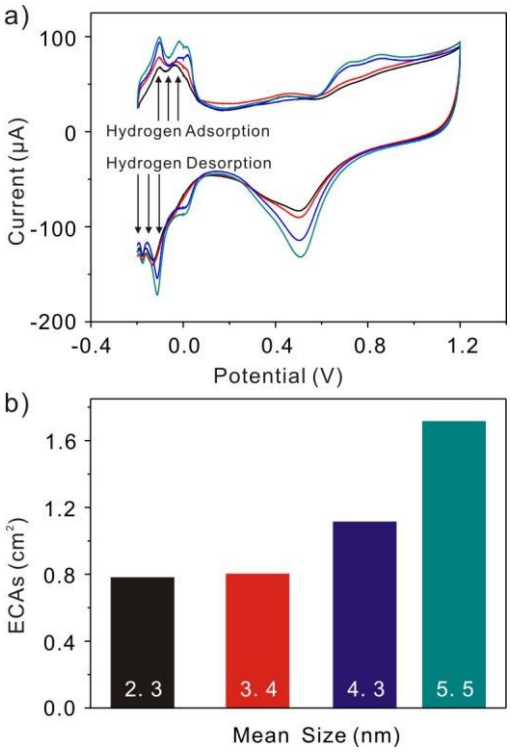

Fig. 6

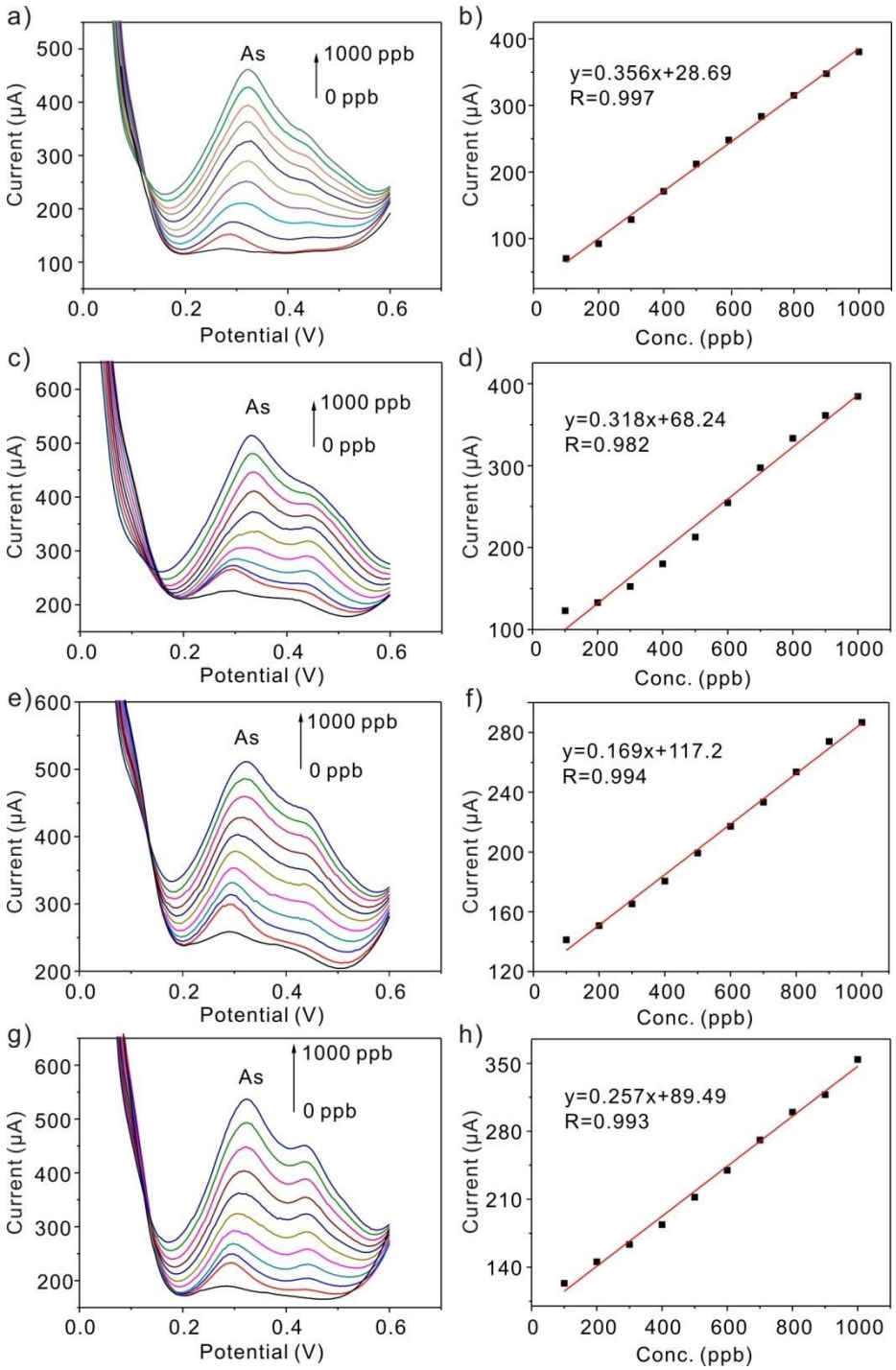

Fig.7

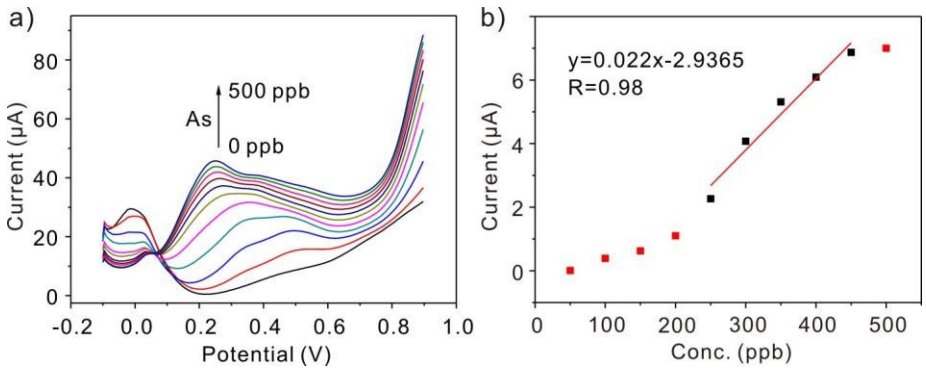

Fig.8

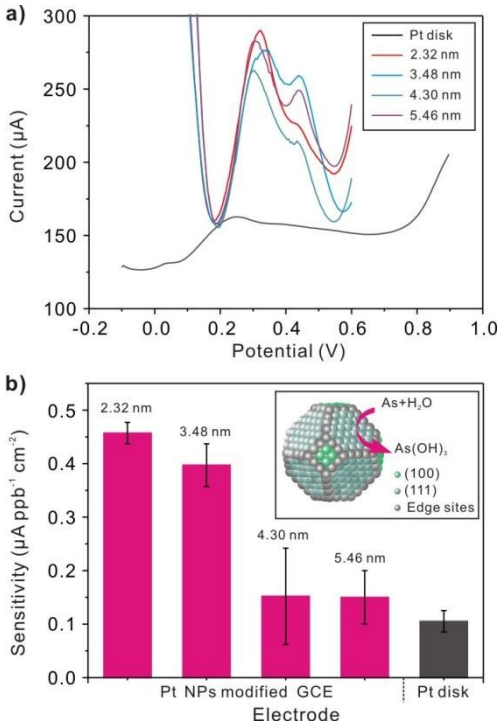

Fig. 9